Observed drought indices show divergence across Europe

Stagge, James H.; Kingston, DG; Tallaksen, Lena M.; Hannah, David M.

DOI:
10.1038/s41598-017-14283-2

Document Version
Peer reviewed version

Citation for published version (Harvard):
Stagge, JH, Kingston, DG, Tallaksen, LM & Hannah, DM 2017, 'Observed drought indices show divergence across Europe', *Scientific Reports*, vol. 7, no. 1, 14045. https://doi.org/10.1038/s41598-017-14283-2

Observed drought indices show increasing divergence across Europe

James H. Stagge[1,*], Daniel G. Kingston[2], Lena M. Tallaksen[1], and David M. Hannah[3]

[1]University of Oslo, Department of Geosciences, Oslo, Norway
[2]University of Otago, Department of Geography, Dunedin, New Zealand
[3]University of Birmingham, Department of Geography, Earth and Environmental Sciences, Birmingham, United Kingdom
[*]Correspondence: James H. Stagge, Department of Civil and Environmental Engineering, Utah State University, 4110 Old Main Hill, Logan, Utah 84321-4110, USA, Email: james.stagge@usu.edu

ABSTRACT

Recent severe European droughts raise the vital question: are we already experiencing measurable changes in drought likelihood that agree with climate change projections? The plethora of drought definitions compounds this question, requiring instead that we ask: how have various types of drought changed, how do these changes compare with climate projections, and what are the causes of observed differences? To our knowledge, this study is the first to reveal a regional divergence in drought likelihood as measured by the two most prominent meteorological drought indices: the Standardized Precipitation Index (SPI) and the Standardized Precipitation-Evapotranspiration Index (SPEI) across Europe over the period 1958-2014. This divergence is driven primarily by an increase in temperature from 1970-2014, which in turn increased reference evapotranspiration (ET_0) and thereby drought area measured by the SPEI. For both indices, Europe-wide analysis shows increasing drought frequencies in southern Europe and decreasing frequencies in northern Europe. Notably, increases in temperature and ET_0 have enhanced droughts in southern Europe while counteracting increased precipitation in northern Europe. This is consistent with projections under climate change, indicating that climate change impacts on European drought may already be observable and highlighting the potential for discrepancies among standardized drought indices in a non-stationary climate.

Introduction

The IPCC report on extreme events and disasters[1] cites a greater uncertainty in capturing recent drought trends compared to other natural hazards. At the global scale, studies have shown either increases or negligible changes in meteorological drought[2–4]. Southern Europe is considered a hot-spot for drought change under climate change[5–9]. While some pan-European studies have identified a slight increase in drought area for the continent[10], continental scale trend studies have partially been confounded by the distinct north-south dipole that yields decreased drought frequency in northern Europe and an increase for southern Europe[6,11,12]. Therefore, results are contingent on the geographical domain, which can shift spatially-averaged values for 'Europe'. Another major source of uncertainty is due to differences in drought index formulation, data sources, and selected time period[3,13–16].

The Standardized Precipitation Index (SPI,[17,18]) and SPEI (Standardized Precipitation-Evapotranspiration Index,[19]) normalize precipitation and climatic water balance (precipitation minus ET_0), respectively, accumulated over a given number of months. The SPI has become widely used because of its low data requirements, ease of statistical interpretation, and recommendation by the WMO[20,21]. However, the SPI is based solely on precipitation, and thus ignores the role of evaporative loss in the terrestrial water balance. In recognition of this limitation, the SPEI was developed as a complementary drought index, to provide a more complete measure of the climate inputs and losses related to drought. The incorporation of ET_0, and by implication temperature, in the SPEI calculation has been hypothesized to capture better the projected and observed effects of climate change[19,22,23]; however, this hypothesis has yet to be tested at the continental scale.

Given this research context, we test herein the hypothesis that two closely related drought indices tracked by most drought warning systems, the SPI and SPEI at 6-month resolution (henceforth SPI6 and SPEI6), produce different drought trends across Europe during the recent past. This work builds on prior studies of observed drought and climate trends in Europe[2–4,10,22,24], providing greater detail and a specific analysis of spatial and temporal divergence between two drought indices in Europe during the last 60 years (1958-2014). Notably, we identify the timing of an increasing deviation between the indices from the late 1980s onwards. We seek to understand the core causes of this deviation by mapping spatial patterns of change, identifying the critical climate variables driving change, and verifying the robustness of findings to methods of calculating ET_0 (used in the SPEI6). We conclude that observed drought trends in Europe are driven by the north-south dipole in precipitation,

superimposed on a Europe-wide increasing trend in reference evapotranspiration, driven by increasing temperatures. These broad trends mirror projections of future drought, providing clear evidence that climate change is already affecting European drought frequency, while also raising a warning that related standardized indices may diverge in a non-stationary climate.

Results

Continental Drought Trends

Observed trends in percent European drought area, i.e. the area fraction of grid cells in drought, were calculated based on the SPI6, SPEI6, along with the difference in percent drought area, A_{DIFF6} (A_{SPEI6} minus A_{SPI6}). For this study, drought was defined as SPI6 or SPEI6 below the 20th percentile for each grid cell separately. Long-term trends for these three variables were modeled by non-linear regression using cubic splines along with variables that controlled for recurrent seasonal cycles, temporal autocorrelation, and bias between the two source data sets: the Watch Forcing Data[25] (WFD, 1958-2001) and the Watch Forcing Data Era-Interim[26] (WFDEI, 1979-2014). These datasets are based on the well-reviewed ERA-40[27] and ERA-Interim[28] gridded climate data, respectively, but have undergone spatial interpolation to improve the resolution to 0.5x0.5°, and been subject to additional validation against observed climate records and bias correction based on rain gauge data[26]. Using overlapping datasets with a bias intercept increases trend confidence during the common time period (1979-2001) and permits calculation of a common trend spanning the full period (1958-2014). Fig. 1 shows A_{SPI6}, A_{SPEI6}, and A_{DIFF6} for both the WFD and WFDEI after accounting for bias, confirming good agreement between the datasets.

The difference between European drought area measured by SPEI and SPI, A_{DIFF6}, shows a statistically significant trend beginning in the late 1980s that continued until 2014 (Fig. 1A). The trend became non-significant towards the end of the period due to increased uncertainty related to its estimation near the end of the record rather than any marked change in slope. The spline trend indicates a difference in drought area measured by the two indices of -0.4% in 1987, which rose to a maximum of 7.1% in 2014, implying that an additional 7.1% of the European land mass would be considered in drought, if drought were defined by climatic water balance (SPEI) rather than precipitation (SPI) alone. This increase was continuous, with an average increase of 2.8% per decade, and shows no signs of slowing or changing direction. The maximum observed, unsmoothed value of A_{DIFF6} occurred in September of 2006 (19.8%), when A_{SPI6} was near the expected mean of 20% based on the drought definition threshold, whereas A_{SPEI6} showed a relatively severe drought, encompassing 33.5% of Europe. A similar A_{DIFF6} trend and onset was observed when the E-Obs dataset[29] was processed by the authors using the same method, lending further confidence to this finding.

Prior to the start of the near-linear increase during the late 1980s, the two drought indices were closely related, with most differences in drought area attributable to noise superimposed onto minor decadal patterns. The monthly difference between A_{SPEI6} and A_{SPI6} alternated between a slightly positive period (1958-1976, $\overline{A}_{DIFF6} = +1.00\%$) and a slightly negative period (1976-1985, ($\overline{A}_{DIFF6} = -1.33\%$). The shift from positive ($A_{SPI6} > A_{SPEI6}$) to negative ($A_{SPI6} < A_{SPEI6}$) occurred rapidly following the longest drought in the record (1975-1976, Fig. 1A). Representation of this step-change by the spline method was as a short, but statistically significant decreasing trend (Fig. 1A). Ultimately, the trends prior to the onset of significant deviation in the late 1980s were minor, indicating that differences between the indices were stable and randomly distributed, especially when compared to the more severe and continuous trend during the past three decades.

To understand the cause of increasing differences in drought area, we considered the trends in A_{SPI6} and A_{SPEI6} separately. These trends clearly show that the observed deviation was mainly caused by significant decreases in SPI-based drought area (A_{SPI6}) (Fig. 1B). The smoothed trend of A_{SPI6} decreased from 22.3% in Jan 1958 to 16.4% in Dec 2014, or -1.04% per decade. Unlike precipitation-based drought area (A_{SPI6}), water balance drought area (SPEI) did not change significantly during this period, increasing only slightly from 20.6% to 21.1% (Fig. 1C).

Spatial Drought Trends

Analysis of continental drought trends show that the total area experiencing SPI6 drought in Europe has decreased significantly during the past 56 years (Fig. 1B), which appears contradictory to previous studies[4,10]. To understand this result, it is vital to analyze consistent spatial patterns in drought trends. Linear trends for each 0.5x0.5° grid cell were calculated using the binary occurrence (presence/absence) of drought within the cell. Drought occurrence was defined in the same manner as for the European scale, i.e. the 20th percentile. In this way, trends in drought occurrence at the grid scale were calculated in an analogous manner to the previous trends in drought area, or the area-weighted sum of binary occurrences across Europe. Trends in drought occurrence were constrained to be linear and presented as the rate of change in drought likelihood (%) per decade, k_{SPI6} and k_{SPEI6}.

Spatial patterns in drought occurrence measured by the SPI6 are broadly similar to those measured by the SPEI6, with increasing occurrence across southern Europe and the Mediterranean and decreasing occurrence for much of northern Europe (Fig. 2A and B). In southern Europe and the Mediterranean, drought likelihood has increased at a rate greater than 3% per decade, which is statistically significant based on a t-test of the trend's slope. For perspective, a 3% increase per decade

would increase drought likelihood from 12% in 1958 to 29% in 2014, assuming it passed through the theoretical mean at the reference period mid-point (1985). The most substantial increase in drought frequency occurred in northern Italy, which experienced no detectable SPI6 droughts prior to 1980 followed by frequent, severe droughts throughout the early 1990s and again in 2003 and 2006-07. In contrast, much of northern Europe experienced significantly decreasing drought likelihood since 1958, particularly when measured by the SPI6 (Fig. 2A and B). The most significantly decreasing drought trends occurred in Latvia (-8.35%/decade) and Scotland (-8.60%/decade) for SPI6 and SPEI6, respectively. Some isolated regions do not strictly adhere to the north-south dipole, such as eastern Turkey and northern Russia; however, these regions have been previously identified[24,26,31] as producing anomalous climate trends, potentially related to low station density, individual gauge issues, or missing data.

The identification of opposing drought trends for northern and southern Europe supports similar findings of a north-south European dipole[10,12,32]. Our results add confidence to these previous findings by applying a more robust regression method that controls for recurrent seasonal patterns and temporal autocorrelation. Notably, our results also closely resemble climate model projections of precipitation that show a drier Mediterranean region and wetter northern Europe[6,33–35]. In this way, our findings place past drought observations firmly into the projected timeline and spatial pattern of European drought impacts due to climate change.

Spatial analysis further highlights the differing trends between the two drought indices and explains why A_{SPI6} decreased during the study period, in apparent conflict with previous studies. A_{SPI6} considers Europe as a whole, integrating the opposed increasing and decreasing drought trends by area weighting. So, despite significant increases in drought likelihood for southern Europe, the greater total area in the north outweighs these trends, resulting in an overall decrease in SPI6 drought frequency and no change in SPEI6 frequency. This is further confirmed by comparing the distribution of k_{SPI6}, with a mean trend of -1.13%/decade, to the distribution of k_{SPEI6}, which is centered around zero, despite highly positive trends, shown by positively-skewed distributions of both indices (Fig. 2).

Unlike the north-south dipole of drought trends, the difference , k_{DIFF6}, between trends measured by the two indices (i.e. k_{SPEI6} - k_{SPI6}) is almost entirely positive across Europe (Fig. 2C). This means that considering ET_0 increases the relative likelihood of drought by an average of 0.97%/decade (95% range of -1.5-5.9%/decade) regardless of location, which is then overlain on the north-south patterns of increasing and decreasing precipitation-based drought. Thus, in regions with a decrease in precipitation-based drought likelihood, such as Germany, inclusion of ET_0 shifts this trend to become positive. In regions near the Mediterranean that already show an increase in precipitation-based drought likelihood, inclusion of ET_0 exacerbates the observed trend.

Trends in Evapotranspiration Components

Because ET_0 represents the primary difference between the SPI and SPEI indices, it is critical to verify the role of ET_0 in the resulting drought trends, to test the sensitivity of the results to ET_0 calculation methods, and to identify the specific climate components that drive the increasing deviation between A_{SPEI6} and A_{SPI6}. ET_0 is calculated in this study by the Penman-Montieth equation using the Hargreaves' simplification for daily radiation[36]. This follows the recommendations given in FAO-56 ([37], Eq. 50), using diurnal temperature difference ($T_{max} - T_{min}$) as a proxy for daily solar radiation, while also considering the direct effects of mean daily temperature and wind speed.

Trends in ET_0, as well as other constituent climate variables, were calculated using the same non-linear regression techniques as for drought area (Fig. 3. The resulting trend in 6-month European ET_0 anomaly has a nearly identical shape to A_{DIFF6} (Fig. 3A), which exhibits a step-change decrease in the late 1970s followed by a decade of low ET_0 and a continuous, statistically significant increasing trend beginning in the late 1980s that continued until the end of the study period (2014). The observed steady increase in ET_0 since the late 1980s is supported by other studies that have noted increases in European evapotranspiration during the same time period[38,39], although our results are unique in providing a trend measure for drought occurrence/frequency. It should be noted that any consistent bias between the WFD and WFDEI was accounted for in the regression model using the term β_{Data}, producing overlapping data and trends as shown in Fig. 1. Trends for the evapotranspiration components also have this correction, producing a continuous and overlapping trend; however, Fig. 3 shows the data and trends without this correction for transparency and to highlight potential differences between the datasets.

Several methods exist to calculate ET_0; therefore, the choice of method is critical as it may affect observed trends[16]. To test the robustness of the results to the choice of estimation procedure, we compared our ET_0 trends with those calculated using the more simplistic Hargreaves' equation (which ignores wind speed) and the more complex FAO-56 version of the Penman-Montieth equation (which adds radiation and humidity terms). These results (Fig. 4) confirm that the ET_0 trend is consistent in shape across all models and that the method chosen here is conservative with respect to trend magnitude. The results also point to a notable discontinuity between the WFD and WFDEI time series when using the full Penman-Montieth equation, which produces a difference in ET_0 variance that repeats seasonally (Fig. 4). This discontinuity is due to a previously observed issue in processing downward shortwave radiation to account for monthly aerosol and cloud cover in the WFDEI[26].

Despite this discontinuity, it is important to note that the Penman-Montieth trend using the WFD matches closely all other ET_0 methods until this dataset ends in 2001. Thus, we chose to use the Penman-Montieth equation with a Hargreaves' simplified radiation. It is currently the most complex ET_0 formulation that avoids the discontinuity in radiation and statistical accounting for differing variance, while providing a slightly conservative trend consistent with all other models.

ET_0 represents the hypothetical atmospheric water demand from a fully wetted surface, but is not strictly equivalent to actual evapotranpiration, which is limited by surface water availability. However, ET_0 provides a valuable estimate at the continental-scale where actual evapotranspiration is challenging to calculate and has a value of its own, particularly for the fully humid climate of Europe and when values are normalized, as in the SPEI.

The three major climate components of ET_0 in this study, daily T_{mean}, T_{max}-T_{min}, and wind speed, each contributes differently to the observed ET_0 trend and ultimately, to the deviation between SPEI6 and SPI6. Mean daily temperature is the primary driver of increasing ET_0, showing a significant increasing trend that begins in early 1979 and continues until 2014 (Fig. 3B). During this period, the overall increase in the smoothed six month T_{mean} anomaly is 1.4° C, or 0.39° C per decade, producing the highest T_{mean} anomaly in 2014 (Fig. 3B). Mean temperature anomalies since 2000 rarely fell below 0° C, the median value during the reference period, supporting the statistically significant trend towards higher temperatures, and thereby higher reference evapotranspiration, in the latter part of the time series. Such an increase is consistent with observed temperature change across the continent during this time period[24,31,40] as well as with climate change projections of continental temperature increases[33,35].

Wind speed and diurnal temperature difference produce secondary effects within the ET_0 trend. Mean European wind speed has no statistically significant long-term trend (Fig. 3C); but it does explain the consistent bias between the WFD and WFDEI datasets (see Methods section for details regarding controlling for bias in regression). The difference between WFD and WFDEI wind speed has been noted previously[28] and is a function of methodological differences between the underlying ERA-40 and ERA-Interim climate data. After removing this bias, there is a minor peak in wind speed during the 1970s followed by a slight decrease, which may be related to global stilling[41]; however, the trend is not significant, implying that wind speed most likely plays a minor role in the observed deviation between A_{SPEI6} and A_{SPI6}. Diurnal temperature difference, T_{max}-T_{min}, used as a proxy for daily solar radiation, underwent a statistically significant step-change decrease between 1967 and 1980 (Fig. 3D). The 1970s step-change corresponds to a decrease in ET_0 during the same period, delaying the effect of already increasing mean temperatures and thereby causing a temporary decrease in A_{DIFF6}. The downturn in diurnal temperature range during this period has been noted in other studies[42,43] and has been linked to a shift from a period of global dimming to a period of global brightening[44] or to shifts in large scale circulation patterns[45].

Implications

This paper reveals, for the first time, an increasing deviation in European regional drought area and frequency measured by two prominent and related drought indices (SPI and SPEI). This divergence is driven primarily by an increase in temperature from 1979 until 2014, which produced a consistent increase in ET_0, delayed until the late 1980s by the secondary effects of a step-change in diurnal radiation. Both the SPI and SPEI indicate that drought frequency has increased in southern Europe and decreased in northern Europe. However, the inclusion of reference evapotranspiration in the SPEI, driven by a steady increase in European temperature, explains the index divergence, enhanced SPEI droughts in the south, and a northward shift of increased drought frequency over time. A northward shift of water balance drought has important implications for future water management and European agriculture[46].

This continental-scale disparity in wetting and drying combined with the rapid onset and continuously increasing deviation is highly consistent with both the timeline and spatial pattern of projected climate change impacts for Europe. Further, it is consistent with findings for precipitation and evapotranspiration divergences at a global scale[47]. This suggests that observations and predictions have converged and also supports the claim that climate change has already produced measurable effects on European drought. These exploratory results provide valuable observations of an observable climate change imprint on European drought occurence and will hopefully motivate attribution studies like[48],[49] to focus on the growing divergence between SPI and SPEI-based drought. Detection of this subtle, but critical deviation among two of the most used meteorological drought metrics highlights the challenge and importance of considering drought trends in a non-stationary climate, particularly when communicating changes in drought risk to stakeholders and policy makers.

Methods

Drought Indices

SPI[17,18] and SPEI[19] were calculated following the method outlined in[50], using a six month accumulation period and one month time step. A six month accumulation period was selected to model seasonal droughts and to reduce the influence of snowmelt timing. SPI6 and SPEI6 were generated for each 0.5° x 0.5° grid cell individually. Normalization was always relative to the

WFD during the reference period 1/1/1971 to 12/31/2000 so that results for the WFD and WFDEI are comparable directly, while also fitting the WMO standard for 30-year climate normals. Normalization of the precipitation-based (SPI) and climatic water balance (SPEI) is based on the two-parameter gamma distribution and Generalized Extreme Value (GEV) distribution, respectively, following recommendations in[50]. Drought indices were calculated separately for WFD and WFDEI to avoid artificially merging the climate data sets and to highlight potential differences in findings based on their slightly different underlying atmospheric models.

Climate Data

All climate data used in this study is based on the Watch Forcing Data (WFD)[25] and the Watch Forcing Data Era-Interim (WFDEI)[26], which cover the periods 1/1/1958-12/31/2001 and 1/1/1979-12/31/2014, respectively. These datasets are based on the well-reviewed ERA-40[27] and ERA-Interim[28] gridded climate data, respectively, but have undergone spatial interpolation to improve the resolution to 0.5x0.5°, while undergoing additional validation against observed climate records[26] and bias correction based on gauge data. Bias correction is based on CRU monthly data, with the WFD correction based on CRU TS2.1 and the WFDEI based on CRU TS3.1, TS3.101, and TS3.21[51].

Precipitation is calculated as the sum of rainfall and snowfall, whereas ET_0 is calculated by the Penman-Montieth Equation using the Hargreaves' simplification to derive solar radiation from the diurnal difference between maximum and minimum temperature ($T_{max} - T_{min}$) ([37] , eq. 50). Calculation of reference evapotranspiration otherwise follows the FAO-56 Penman-Montieth method[37]. It should be noted that reference evapotranspiration is not equivalent to actual evapotranspiration, which is limited by surface water availability. The Hargreaves' simplification was used to avoid a previously discovered discontinuity between the WFD and WFDEI downward shortwave radiation[26] that affected the full FAO-56 Penman-Montieth equation ([37] , eq. 6). Sensitivity of the results to the ET_0 methodology was quantified by comparing ET_0 calculated using the FAO-56 equation with Hargreaves' radiation simplification to the more complex, full FAO-56 equation and simpler Hargreaves' equation[36]. Use of the FAO-56 equation with Hargreaves' radiation was found to be reasonable and conservative, representing the most complex ET_0 formulation that also avoids issues with the WFD/WFDEI radiation discrepancy.

Drought Trend Analysis

Analysis is divided into three steps. First, separate trends in percent European drought area were calculated based on the SPI6, SPEI6, and the difference between their drought area. Then, trends in SPI6 and SPEI6 drought occurrence were determined for each grid cell, allowing for a spatial comparison of trend patterns. Finally, trends in the constituents of SPEI across the European domain were tested to determine the role of each component in explaining the observed differences between SPI6 and SPEI6.

For the purposes of this study, Europe is defined by the domain (-10° to 48° E) by (33° to 72° N). Iceland and the Azores are not included in this definition of Europe. A cell is considered to be in drought if the SPI6 or SPEI6 $<$ -0.84, corresponding to the 20th percentile. Thus, European drought area is the percent area below this threshold. In addition to calculating the percent drought area for SPI6 and SPEI6, referred to as A_{SPI6} and A_{SPEI6}, respectively, the difference in drought area estimated by these two indices was calculated as

$$A_{DIFF6} = A_{SPEI6} - A_{SPI6} \tag{1}$$

Trends in A_{SPI6} and A_{SPEI6} were calculated by using a logit link, $\text{logit}(\pi_i) = ln\left(\frac{\pi_i}{1-\pi_i}\right)$, which models the proportion of binary occurrences, π_i, between 0 to 100%. Because A_{DIFF6} is instead bounded by -100% and 100%, trends in A_{DIFF6} were calculated using a standard Gaussian model. Each trend was fit using the general equation:

$$\text{logit}(A_{SPI6}) = f_{Trend}(\text{Date}) + f_M(\text{Month}) + \beta_{Data} + \beta_0 + \varepsilon_t \tag{2}$$

$$\text{where} \quad \varepsilon_t = \sum_{n=1}^{n=3} \phi_n \varepsilon_{t-n} + u_t \tag{3}$$

in which $f_{Trend}(\text{Date})$ represents a spline curve response to the calendar date between 1/1/1958 and 12/31/2014, $f_M(\text{Month})$ is a 12 month cyclic cubic spline constrained to ensure continuity across each new year, β_{Data} is an intercept that accounts for differences between the WFD and WFDEI, β_0 is the model intercept, and ε_t is a term that can account for temporal autocorrelation among the model errors. Autocorrelation is modeled by an AR term of 1-3 month lags, defined by $\phi_n \varepsilon_{t-n}$ where n is the AR month lag. In this way, $f_{Trend}()$ measures a long-term trend in A_{SPI6} without imposing a linear requirement, while the remainder of the model accounts for other patterns and factors that could affect the trend term. All non-significant terms were removed from the final model. Regression fitting was performed using the mgcv package in R[52].

Trends for A_{DIFF6} were calculated by a similar approach, using a Gaussian model rather than the logit transform:

$$A_{DIFF6} = f_{Trend}(\text{Date}) + f_M(\text{Month}) + \beta_{Data} + \beta_0 + \varepsilon_t \quad (4)$$

$$\text{where} \quad \varepsilon_t = \sum_{n=1}^{n=3} \phi_n \varepsilon_{t-n} + u_t \qquad u_t = N(0, \sigma^2) \quad (5)$$

Trend significance was calculated by determining whether the instantaneous first derivative of the $f_{Trend}()$ spline term was significantly different from zero using a t-test with $\alpha = 5\%$.

Spatial trends were calculated by a similar model, but instead used the binary occurrence of drought at each grid cell rather than the percent area across Europe. The regression model therefore used logistic regression, but assumed a linear trend for each grid cell to allow for easier comparisons of trend slopes:

$$\text{logit}\,(\pi_{SPI6<-0.84}) = k_{SPI6}(\text{Date}) + f_M(\text{Month}) + \beta_{Data} + \beta_0 + \varepsilon_t \quad (6)$$

$$\text{where} \quad \varepsilon_t = \sum_{n=1}^{n=3} \phi_n \varepsilon_{t-n} + u_t \quad (7)$$

where k_{SPI6} is the long-term trend for the SPI6 drought likelihood. This trend in likelihood is presented as a percent change in drought occurrence per decade. Long-term differences between SPI6 and SPEI6 drought trends at the grid cell resolution are calculated by subtracting trends in drought occurrence for each variable:

$$k_{DIFF6} = k_{SPEI6} - k_{SPI6} \quad (8)$$

where k is the trend in drought likelihood and subscripts refer to the drought index or the difference between their likelihoods. Statistical significance was calculated for k_{SPI6} and k_{SPEI6} using a t-test of the trend's slope, while the statistical significance of k_{DIFF6} was calculated following[53].

Trends in the constituent climate variables were determined by first calculating the 6-month seasonal anomaly for each variable: ET_0, T_{mean}, T_{max}, T_{min}, $T_{max} - T_{min}$, and 2 m wind speed. This involved calculating the six month moving average for each constituent at each grid cell and subtracting the seasonal mean using the same reference period as defined for the SPI and SPEI. The seasonal anomaly for Europe was then calculated as the area-weighted mean of these anomalies. In this way, seasonal anomalies are handled in exactly the same manner as SPI and SPEI, making them comparable. Trends were then calculated using the same Gaussian models described in Equations 4-5.

References

1. IPCC. *Managing the Risks of Extreme Events and Disasters to Advance Climate Change Adaptation. A Special Report of Working Groups I and II of the Intergovernmental Panel on Climate Change (IPCC) [Field, C. B., V. Barros, T. F. Stocker, D. Qin, D. J. Dokken, K. L. Ebi, M. D. Mastrandrea, K. J. Mach, G.-K. PLattner, S. K. Allen, M. Tignor, and P. M. Midgley (eds.)]* (Cambridge University Press, Cambridge, United Kingdom and New York, NY, USA, 2012).
2. Dai, A. Increasing drought under global warming in observations and models. *Nat. Clim. Chang.* **3**, 52–58; DOI: 10.1038/nclimate1633 (2013).
3. Sheffield, J., Wood, E. F. & Roderick, M. L. Little change in global drought over the past 60 years. *Nat.* **491**, 435–438; DOI: 10.1038/nature11575 (2012).
4. Burke, E. J., Brown, S. J. & Christidis, N. Modeling the Recent Evolution of Global Drought and Projections for the Twenty-First Century with the Hadley Centre Climate Model. *J. Hydrometeorol.* **7**, 1113–1125; DOI: 10.1175/JHM544.1 (2006).
5. Sheffield, J. & Wood, E. F. Projected changes in drought occurrence under future global warming from multi-model, multi-scenario, IPCC AR4 simulations. *Clim. Dyn.* **31**, 79–105; DOI: 10.1007/s00382-007-0340-z (2007).
6. Orlowsky, B. & Seneviratne, S. I. Elusive drought: uncertainty in observed trends and short- and long-term CMIP5 projections. *Hydrol. Earth Syst. Sci.* **17**, 1765–1781; DOI: 10.5194/hess-17-1765-2013 (2013).
7. Dubrovský, M. *et al.* Multi-GCM projections of future drought and climate variability indicators for the Mediterranean region. *Reg. Environ. Chang.* **14**, 1907–1919; DOI: 10.1007/s10113-013-0562-z (2014).

8. Stagge, J. H., Rizzi, J., Tallaksen, L. M. & Stahl, K. Future Meteorological Drought Projections of Regional Climate. Tech. Rep. 25, DROUGHT-R&SPI Project (2015).

9. Spinoni, J., Naumann, G. & Vogt, J. Spatial patterns of European droughts under a moderate emission scenario. *Adv. Sci. Res.* **12**, 179–186; DOI: 10.5194/asr-12-179-2015 (2015).

10. Bordi, I., Fraedrich, K. & Sutera, A. Observed drought and wetness trends in Europe: an update. *Hydrol. Earth Syst. Sci.* **13**, 1519–1530; DOI: 10.5194/hess-13-1519-2009 (2009).

11. Spinoni, J., Naumann, G., Vogt, J. & Barbosa, P. European drought climatologies and trends based on a multi-indicator approach. *Glob. Planet. Chang.* **127**, 50–57; DOI: 10.1016/j.gloplacha.2015.01.012 (2015).

12. Spinoni, J., Naumann, G. & Vogt, J. V. Pan-European seasonal trends and recent changes of drought frequency and severity. *Glob. Planet. Chang.* **148**, 113–130; DOI: 10.1016/j.gloplacha.2016.11.013 (2017).

13. Seneviratne, S. I. Historical drought trends revisited. *Nat.* **491**, 338–339; DOI: 10.1038/491338a (2012).

14. Dubrovsky, M. *et al.* Application of relative drought indices in assessing climate-change impacts on drought conditions in Czechia. *Theor. Appl. Climatol.* **96**, 155–171; DOI: 10.1007/s00704-008-0020-x (2009).

15. Hannaford, J., Buys, G., Stahl, K. & Tallaksen, L. M. The influence of decadal-scale variability on trends in long European streamflow records. *Hydrol. Earth Syst. Sci.* **17**, 2717–2733; DOI: 10.5194/hess-17-2717-2013 (2013).

16. Trenberth, K. E. *et al.* Global warming and changes in drought. *Nat. Clim. Chang.* **4**, 17–22; DOI: 10.1038/nclimate2067 (2014).

17. McKee, T. B., Doesken, N. J. & Kleist, J. The relationship of drought frequency and duration to time scales. vol. 17, 179–183 (American Meteorological Society Boston, MA, 1993).

18. Guttman, N. B. Accepting the Standardized Precipitation Index: A Calculation Algorithm. *JAWRA J. Am. Water Resour. Assoc.* **35**, 311–322; DOI: 10.1111/j.1752-1688.1999.tb03592.x (1999).

19. Vicente-Serrano, S. M., Beguería, S. & López-Moreno, J. I. A multi-scalar drought index sensitive to global warming: the standardized precipitation evapotranspiration index – SPEI. *J. Clim.* **23**, 1696–1718 (2010).

20. World Meteorological Organization (WMO) & Global Water Partnership (GWP). *Handbook of Drought Indicators and Indices [Svoboda, M., and B. A. Fuchs (eds.)]* (Integrated Drought Management Programme (IDMP), Geneva, 2016).

21. Hayes, M., Svoboda, M., Wall, N. & Widhalm, M. The Lincoln Declaration on Drought Indices: Universal Meteorological Drought Index Recommended. *Bull. Am. Meteorol. Soc.* **92**, 485–488; DOI: 10.1175/2010BAMS3103.1 (2011).

22. Vicente-Serrano, S. M. *et al.* Evidence of increasing drought severity caused by temperature rise in southern Europe. *Environ. Res. Lett.* **9**, 044001; DOI: 10.1088/1748-9326/9/4/044001 (2014).

23. Touma, D., Ashfaq, M., Nayak, M. A., Kao, S.-C. & Diffenbaugh, N. S. A multi-model and multi-index evaluation of drought characteristics in the 21st century. *J. Hydrol.* **526**, 196–207; DOI: 10.1016/j.jhydrol.2014.12.011 (2015).

24. van der Schrier, G., van den Besselaar, E. J. M., Klein Tank, A. M. G. & Verver, G. Monitoring European average temperature based on the E-OBS gridded data set. *J. Geophys. Res. Atmospheres* **118**, 5120–5135; DOI: 10.1002/jgrd.50444 (2013).

25. Weedon, G. P. *et al.* Creation of the WATCH Forcing Data and Its Use to Assess Global and Regional Reference Crop Evaporation over Land during the Twentieth Century. *J. Hydrometeorol.* **12**, 823–848; DOI: 10.1175/2011jhm1369.1 (2011).

26. Weedon, G. P. *et al.* The WFDEI meteorological forcing data set: WATCH Forcing Data methodology applied to ERA-Interim reanalysis data. *Water Resour. Res.* **50**, 7505–7514; DOI: 10.1002/2014WR015638 (2014).

27. Uppala, S. M. *et al.* The ERA-40 re-analysis. *Q. J. Royal Meteorol. Soc.* **131**, 2961–3012; DOI: 10.1256/qj.04.176 (2005).

28. Dee, D. P. *et al.* The ERA-Interim reanalysis: configuration and performance of the data assimilation system. *Q. J. Royal Meteorol. Soc.* **137**, 553–597; DOI: 10.1002/qj.828 (2011).

29. Haylock, M. R. *et al.* A European daily high-resolution gridded data set of surface temperature and precipitation for 1950-2006. *J. Geophys. Res.* **113**, D20119; DOI: 10.1029/2008jd010201 (2008).

30. Wickham, H. *ggplot2: Elegant Graphics for Data Analysis* (Springer-Verlag New York, 2009).

31. Nilsen, I. B., Stagge, J. H. & Tallaksen, L. M. A probabilistic approach for attributing temperature changes to synoptic type frequency. *Int. J. Climatol.* **37**, 2990–3002; DOI: 10.1002/joc.4894 (2017).

32. Klein Tank, A. M. G. & Können, G. P. Trends in Indices of Daily Temperature and Precipitation Extremes in Europe, 1946–99. *J. Clim.* **16**, 3665–3680; DOI: 10.1175/1520-0442(2003)016¡3665:TIIODT¿2.0.CO;2 (2003).

33. Christensen, J. H. & Christensen, O. B. A summary of the PRUDENCE model projections of changes in European climate by the end of this century. *Clim. Chang.* **81**, 7–30; DOI: 10.1007/s10584-006-9210-7 (2007).

34. Heinrich, G. & Gobiet, A. The future of dry and wet spells in Europe: a comprehensive study based on the ENSEMBLES regional climate models. *Int. J. Climatol.* **32**, 1951–1970; DOI: 10.1002/joc.2421 (2012).

35. Jacob, D. *et al.* EURO-CORDEX: new high-resolution climate change projections for European impact research. *Reg. Environ. Chang.* **14**, 563–578; DOI: 10.1007/s10113-013-0499-2 (2013).

36. Hargreaves, G. H. & Samani, Z. A. Reference crop evapotranspiration from ambient air temperature. *Am. Soc. Agric. Eng.* (1985).

37. Allen, R., Pereira, L., Raes, D. & Smith, M. Crop evapotranspiration. FAO irrigation and drainage paper 56. *FAO, Rome, Italy* **10** (1998).

38. Zeng, Z. *et al.* Global evapotranspiration over the past three decades: estimation based on the water balance equation combined with empirical models. *Environ. Res. Lett.* **7**, 014026; DOI: 10.1088/1748-9326/7/1/014026 (2012).

39. Teuling, A. J. *et al.* A regional perspective on trends in continental evaporation. *Geophys. Res. Lett.* **36**, L02404; DOI: 10.1029/2008GL036584 (2009).

40. van Oldenborgh, G. J. *et al.* Western Europe is warming much faster than expected. *Clim. Past* **5**, 1–12; DOI: 10.5194/cp-5-1-2009 (2009).

41. McVicar, T. R. *et al.* Global review and synthesis of trends in observed terrestrial near-surface wind speeds: Implications for evaporation. *J. Hydrol.* **416–417**, 182–205; DOI: 10.1016/j.jhydrol.2011.10.024 (2012).

42. Easterling, D. R. *et al.* Maximum and Minimum Temperature Trends for the Globe. *Sci.* **277**, 364–367; DOI: 10.1126/science.277.5324.364 (1997).

43. Makowski, K., Wild, M. & Ohmura, A. Diurnal temperature range over Europe between 1950 and 2005. *Atmos. Chem. Phys.* **8**, 6483–6498; DOI: 10.5194/acp-8-6483-2008 (2008).

44. Wild, M., Ohmura, A. & Makowski, K. Impact of global dimming and brightening on global warming. *Geophys. Res. Lett.* **34**, L04702; DOI: 10.1029/2006gl028031 (2007).

45. Ionita, M., Lohmann, G., Rimbu, N. & Scholz, P. Dominant modes of Diurnal Temperature Range variability over Europe and their relationships with large-scale atmospheric circulation and sea surface temperature anomaly patterns. *J. Geophys. Res. Atmospheres* **117**, D15111; DOI: 10.1029/2011JD016669 (2012).

46. Olesen, J. E. *et al.* Impacts and adaptation of European crop production systems to climate change. *Eur. J. Agron.* **34**, 96–112; DOI: 10.1016/j.eja.2010.11.003 (2011).

47. McCabe, G. J. & Wolock, D. M. Variability and trends in global drought. *Earth Space Sci.* **2**, 2015EA000100; DOI: 10.1002/2015EA000100 (2015).

48. Diffenbaugh, N. S., Swain, D. L. & Touma, D. Anthropogenic warming has increased drought risk in California. *Proc. Natl. Acad. Sci.* **112**, 3931–3936; DOI: 10.1073/pnas.1422385112 (2015).

49. Gudmundsson, L. & Seneviratne, S. I. Anthropogenic climate change affects meteorological drought risk in Europe. *Environ. Res. Lett.* **11**, 044005; DOI: 10.1088/1748-9326/11/4/044005 (2016).

50. Stagge, J. H., Tallaksen, L. M., Gudmundsson, L., Van Loon, A. F. & Stahl, K. Candidate Distributions for Climatological Drought Indices (SPI and SPEI). *Int. J. Climatol.* **35**, 4027–4040; DOI: 10.1002/joc.4267 (2015).

51. Harris, I., Jones, P., Osborn, T. & Lister, D. Updated high-resolution grids of monthly climatic observations – the CRU TS3.10 Dataset. *Int. J. Climatol.* **34**, 623–642; DOI: 10.1002/joc.3711 (2014).

52. Wood, S. N. *Generalized Additive Models: An Introduction with R* (Chapman and Hall/CRC, 2006).

53. Clogg, C. C., Petkova, E. & Haritou, A. Statistical Methods for Comparing Regression Coefficients Between Models. *Am. J. Sociol.* **100**, 1261–1293; DOI: 10.1086/230638 (1995).

Acknowledgements

This study was financially supported by the EU FP7 project DROUGHT-R&SPI (contract no. 282769) and forms a contribution to the UNESCO-IHP FRIEND-Water Programme. The data used are listed in the references and code repository at `https://github.com/jstagge/drought_divergence`

Author contributions statement

J.H.S. and D.G.K. independently identified the diverging trend and conceived the research design together. D.G.K. wrote an initial draft outline and manuscript, while J.H.S. performed the analysis and wrote the finalized manuscript. L.M.T., D.M.H., and D.G.K. edited the manuscript and provided conceptual advice throughout the project.

Additional information

The author(s) declare no competing financial interests.

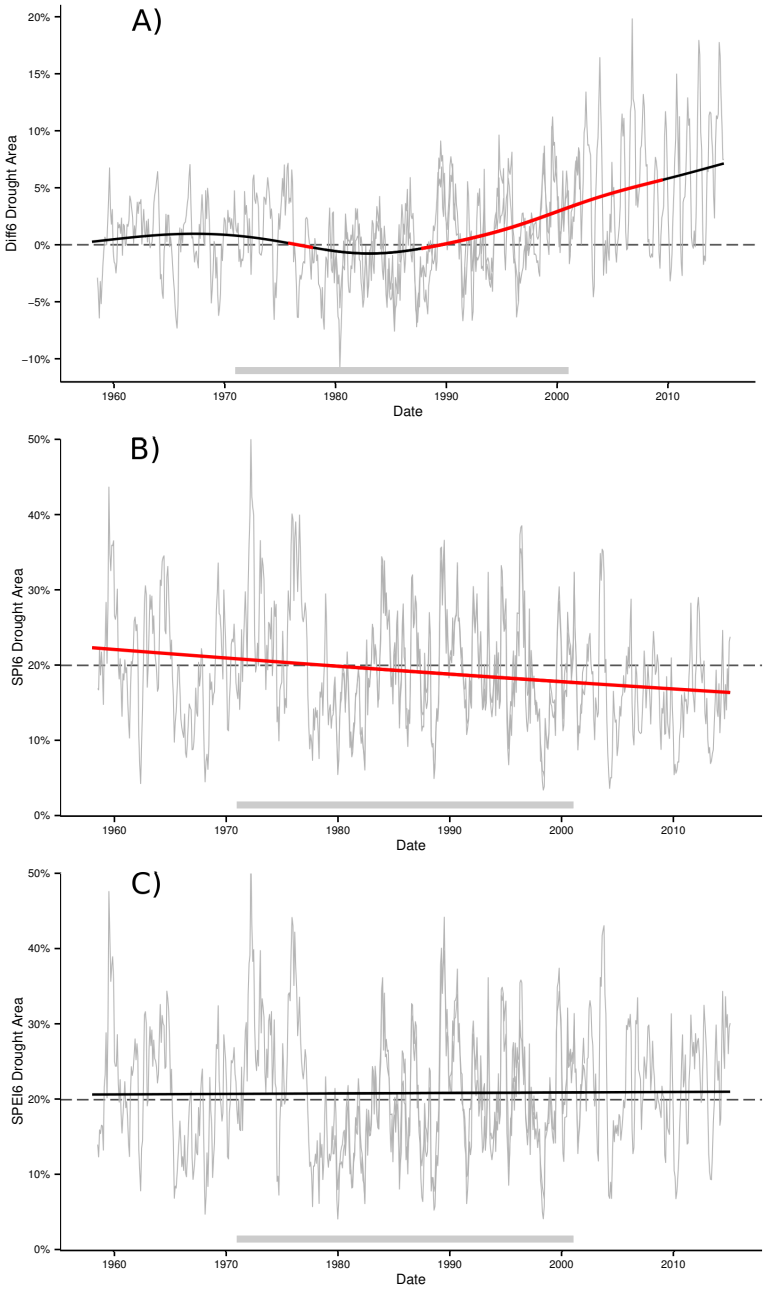

Figure 1. Difference in percent area in drought A_{Diff6} (A), followed by the percent area in drought calculated by (B) SPI6, A_{SPI6}, and (C) SPEI6, A_{SPEI6}. Historical values for both the WFD and WFDEI are shown in grey, while the fitted common trend in shown in black. Statistically significant trends are shown in red. A grey bar at the bottom shows the reference period.

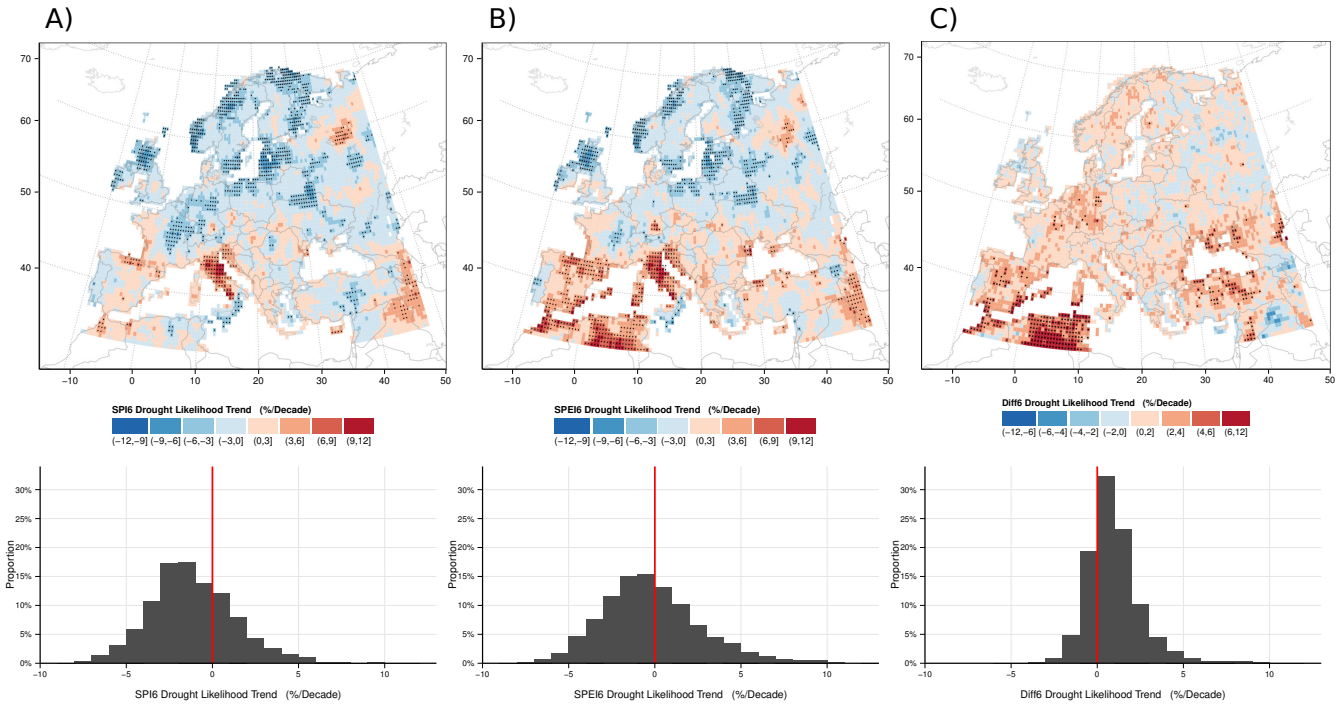

Figure 2. Spatial distribution of (A) k_{SPI6}, (B) k_{SPEI6}, and (C) k_{DIFF6}. Stipples represent statistically significant trends. The distribution of trends for all grid cells is shown below the corresponding map. The color scale for k_{DIFF6} is modified slightly to match its smaller variance. Figure generated using the ggplot2 package[30] in R version 3.4.0. (https://cran.r-project.org/).

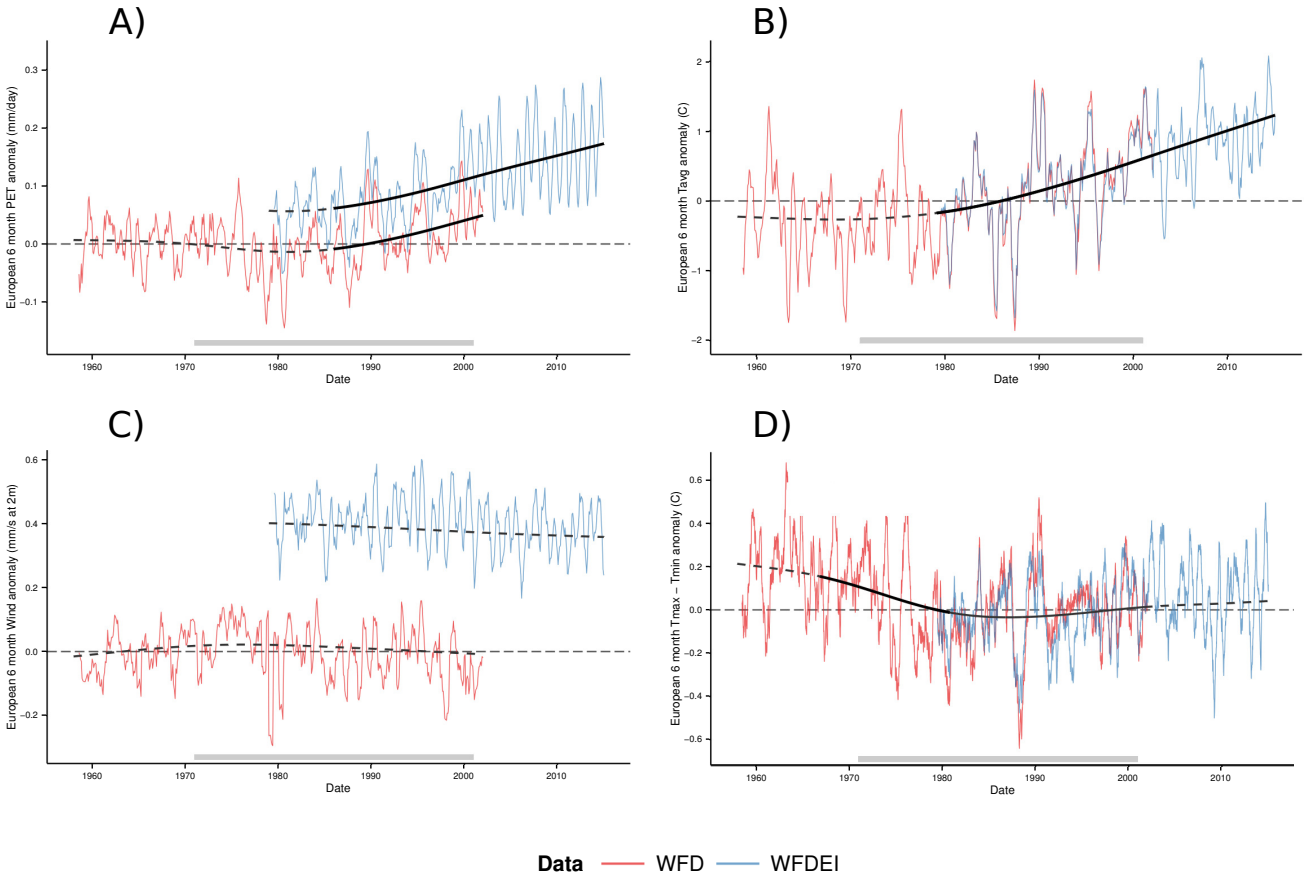

Figure 3. Mean six month seasonal anomaly averaged across Europe for reference evapotranspiration (A) and its constituents: (B) daily T_{Mean}, (C) wind speed, and (D) $T_{Max} - T_{Min}$. Historical data are shown in red (WFD) and blue (WFDEI). No bias correction is included to highlight differences between WFD and WFDEI. Long term trends are shown as a dotted line, with significant trends as a solid, black overlay. A grey bar at the bottom shows the reference period.

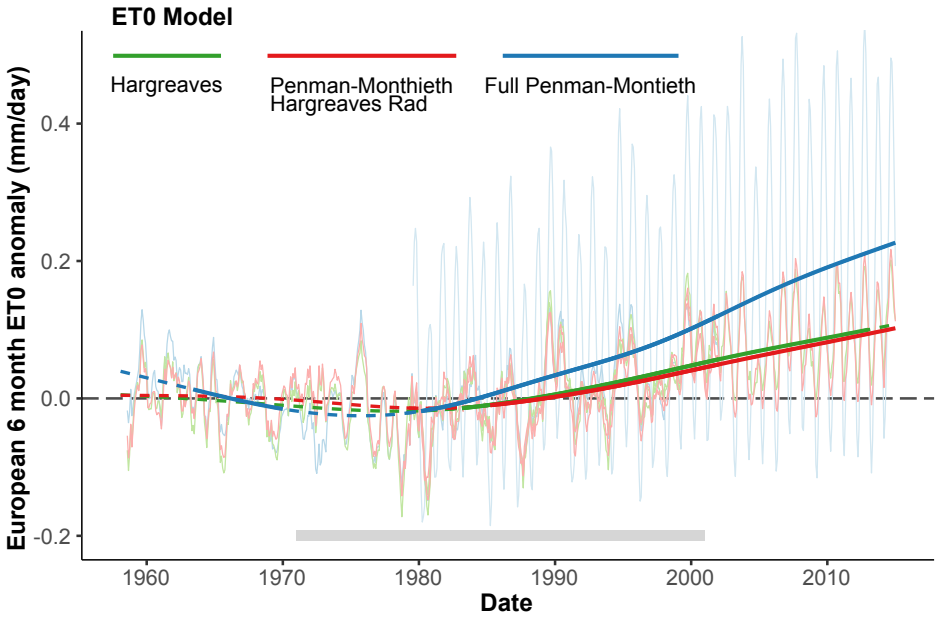

Figure 4. Anomalies in six month mean reference evapotranspiration calculated using three models of increasingly complexity and data requirements. WFD and WFDEI time series are plotted separately in light colors, whereas the spline trend is shown in bold.